Science of the Total Environment 698 (2020) 134245

Contents lists available at ScienceDirect

Science of the Total Environment

journal homepage: www.elsevier.com/locate/scitotenv

Seasonal and diurnal variations of greenhouse gases in Florence (Italy): Inferring sources and sinks from carbon isotopic ratios

S. Venturi [a,b,*], F. Tassi [a,b], J. Cabassi [a,b], B. Gioli [c], S. Baronti [c], O. Vaselli [a,b], C. Caponi [a], C. Vagnoli [c], G. Picchi [a], A. Zaldei [c], F. Magi [a], F. Miglietta [c], F. Capecchiacci [d]

[a] Department of Earth Sciences, University of Florence, Via G. La Pira 4, 50121 Firenze, Italy
[b] Institute of Geosciences and Earth Resources (IGG), National Research Council of Italy (CNR), Via G. La Pira 4, 50121 Firenze, Italy
[c] Institute of Biometeorology (IBIMET), National Research Council of Italy (CNR), Via G. Caproni 8, 50145 Firenze, Italy
[d] INGV Istituto Nazionale di Geofisica e Vulcanologia - Osservatorio Vesuviano, via Diocleziano 328, 80122 Napoli, Italy

HIGHLIGHTS

- Reducing urban greenhouse gas emissions requires recognition of emitting sources.
- Isotopic partitioning method was applied for source identification in Florence.
- Florence acts as a net source of CO_2 resulting from traffic and gas combustion.
- Green infrastructures are not sufficient to counterbalance anthropogenic emissions.
- CH_4 emissions are mostly related to fugitive leakages from natural gas pipelines.

GRAPHICAL ABSTRACT

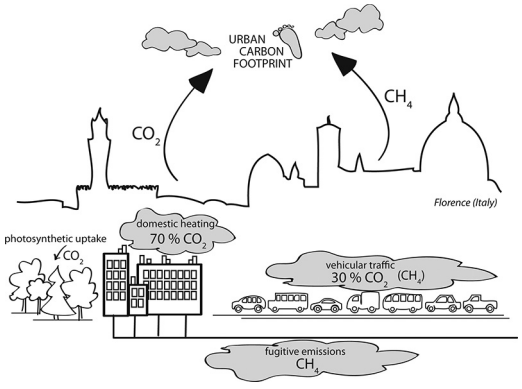

ARTICLE INFO

Article history:
Received 10 June 2019
Received in revised form 11 August 2019
Accepted 1 September 2019
Available online 02 September 2019

Editor: Pavlos Kassomenos

Keywords:
Greenhouse gases
Carbon isotopes
Urban air quality
Cities
Photosynthesis

ABSTRACT

In this study, the results of a continuous monitoring of (i) CO_2 fluxes, and (ii) CO_2 and CH_4 concentrations and carbon isotopic ratios ($\delta^{13}C$-CO_2 and $\delta^{13}C$-CH_4) in air, carried out from 7 to 21 July 2017 and from October 10 to December 15, 2017 in the city centre of Florence, are presented. The measurements were performed from the roof of the historical building of the Ximenes Observatory. CO_2 flux data revealed that the metropolitan area acted as a net source of CO_2 during the whole observation period. According to the Keeling plot analysis, anthropogenic contributions to atmospheric CO_2 were mainly represented by vehicular traffic (about 30%) and natural gas combustion (about 70%), the latter contributing 7 times more in December than in July. Moreover, the measured CO_2 fluxes were about 80% higher in fall than in summer, confirming that domestic heating based on natural gas is the dominant CO_2 emitting source in the municipality of Florence. Even though the continuous monitoring revealed a shift in the $\delta^{13}C$-CO_2 values related to photosynthetic uptake of atmospheric CO_2, the isotopic effect induced by plant activity was restricted to few hours in October and, to a lesser extent, in November. This suggests that urban planning policies should be devoted to massively increase green infrastructures in the metropolitan area in order to counterbalance anthropogenic emissions. During fall, the atmospheric CH_4 concentrations were sensibly higher with respect to those recorded in summer, whilst the $\delta^{13}C$-CH_4 values shifted towards heavier values. The Keeling plot analysis suggested that urban CH_4 emissions were largely related to

* Corresponding author at: Department of Earth Sciences, University of Florence, Via G. La Pira 4, 50121 Firenze, Italy.
E-mail address: stefania.venturi@unifi.it (S. Venturi).

https://doi.org/10.1016/j.scitotenv.2019.134245

fugitive emissions from the natural gas distribution pipeline network. On the other hand, $\delta^{13}C$-CH_4 monitoring allowed to recognize vehicular traffic as a minor CH_4 emitting source.

1. Introduction

The Paris Agreement, signed by 195 countries, *aims to strengthen the global response to the threat of climate change* (Art. 2.1) setting a target for 80% reduction below 1990 levels of global greenhouse gas (hereafter, GHG) emissions by 2050, ensuring zero net global carbon emissions from energy sector by 2060. Actions needed for achieving this ambitious goal require that current plans and policies for renewable energy deployment have to be coordinated with environmental protection projects and interventions. According to Hoornweg et al. (2011), 70% of energy-related GHG emissions can be attributed to urban and suburban activities, where housing and transport sectors account for >50% of direct household emissions of urban citizens (Pichler et al., 2017), with a clear connection between GHG emissions and economic and social urban progress. According to the 2018 Revision of World Urbanization Prospects (United Nations Population Division, 2018), global population living in urban areas is expected to increase from 55% in 2018 to 68% by 2050. Consequently, city administrations and citizens will be in charge of achieving the largest share of GHG emissions reductions. Hence, national policies and local governments are being called to respond to the overlapping challenges of sustainable development, climate change mitigation, and increase of urban resilience (Hoornweg et al., 2011). According to Meerow et al. (2016), urban resilience can be defined as "*the ability of an urban system - and all its constituent socio-ecological and socio-technical networks across temporal and spatial scales - to maintain or rapidly return to desired functions in the face of a disturbance, to adapt to change, and to quickly transform systems that limit current or future adaptive capacity*". Such flexibility should be combined with policies pursuing the achievement of overall urban sustainability, i.e. the establishment of a balance between socioeconomic needs of citizens and the supply of natural resources, preserving the quality of the natural environment by minimizing (and possibly eliminating) the ecological footprint of urban areas (e.g. Huang et al., 2015 and references therein).

Urban planning strategies and local policy initiatives can play a major role in both climate change mitigation and adaptation. Several actions have been successfully implemented by local administrators in several cities aimed at reducing the carbon footprint and amending citizen attitudes towards urban mobility, e.g. promoting public transport services, developing a network of high-quality cycling routes, creating traffic-free zones, establishing congestion taxes or increasing fuel prices and parking fees (Hoornweg et al., 2011; Pichler et al., 2017). Similar initiatives have been adopted by the municipality of Florence, in Tuscany (central Italy), which is the eighth most populous city in Italy, hosting ~380,000 inhabitants. Moreover, it is located in one of the sixth most inhabited metropolitan areas in Italy (about 1,005,000 inhabitants), and is visited by >10 million tourists per year. According to the IRSE regional emission inventory (data are referring to 1995, 2000, 2003, 2005, 2007 and 2010) provided by the Tuscan Regional Government (Regione Toscana, 2010), the annual CO_2 and CH_4 emissions to the atmosphere from Florence city area were estimated to be varying between 1.17×10^6 and 1.34×10^6 Mg and between 1.66×10^3 and 3.12×10^3 Mg, respectively. The CO_2 emissions were mainly ascribed to vehicular traffic (46%) and non-industrial combustion plants, i.e. domestic heating (45%). Only 18% of CH_4 released from the urban area into the atmosphere was related to these sources and mostly attributed to the distribution of fossil fuels (81%) (Regione Toscana, 2010). A similar source partitioning was estimated by Gioli et al. (2012, 2015) for CO_2 (road traffic: 35%; heating: 65%) and CH_4 (road traffic + heating: 14%; gas network leakages: 86%). Nevertheless, in the framework of the ICLEI (International Council for Local Environmental Initiatives) World Congress 2018, the local government has renewed its intent to lower urban CO_2 emissions of 50% by 2030. Accordingly, urban planning strategies in the last ten years have deeply changed the urban area of Florence by (i) pedestrianizing large portions of the city center, (ii) increasing the number of bicycle lanes, and (iii) constructing a tramway network integrated with railway and bus system and a park and ride facility along the most important highway that licks the city. While these efforts are expected to produce environmental benefits, recent monitoring surveys conducted by the environmental protection agency of Tuscany Region (ARPAT, 2018) remarked that Florence is still affected by poor air quality conditions. In order to make intervention plans effectively incisive in reducing urban GHG emissions, a complete inventory of the emitting sources and a regular monitoring activity of atmospheric GHG concentrations are essential prerequisites to allow policymakers to address mitigation efforts and acquire useful tools for evaluating whether GHG emissions are effectively reducing after specific interventions.

In this study, the results of a continuous monitoring (from 7 to 21 July 2017 and from October 10 to December 15, 2017) of (i) CO_2 fluxes, (ii) atmospheric CO_2 and CH_4 concentrations and carbon isotopic ratios ($\delta^{13}C$-CO_2 and $\delta^{13}C$-CH_4) and (iii) meteorological parameters from the rooftop monitoring site of the 250 years old Ximenes Observatory in Florence are presented. The aim was to determine the seasonal and diurnal variations in terms of concentrations and isotopic compositions of these GHG in order to (i) identify the local emitting sources, (ii) establish how the relative contributions were varying with time and (iii) assess the carbon isotopic dynamics of atmospheric CO_2 and CH_4 and the potential of source partitioning methodologies based on isotopic data.

2. Material and methods

2.1. Measurement site

The measurement site was located in the city center of Florence (Firenze; Fig. 1), in central Italy, a city located at about 50 m a.s.l. in an alluvial plain surrounded by sedimentary hills (reaching an altitude of 300–400 m a.s.l.) and crossed by the Arno river and minor creeks. The urban area is characterized by a temperate climate, with mild winters and hot and humid summers. The rainfall pattern shows a minimum in July and a maximum in November, with an annual average rain of about 850 mm.

The instrumental equipment was installed on the roof of the historical building of the Ximenes Observatory (43°47′ N, 11°15′ E; Fig. 1). This astronomical observatory was founded by Leonardo Ximenes in 1756 on the upper floor of the monastery of San Giovannino, ~160 m away from the Santa Maria del Fiore Cathedral and the worldwide renowned Brunelleschi's Dome, which dominates the skyline of the city. Nowadays, the observatory is an independent scientific agency. The roof of the observatory, about 33 m above the street level and 18 m above the average building height, dominates the surrounding buildings with the sole exceptions of the Cathedral's Dome and the Cappella dei Principi, the latter being part of the Medici Chapels, in the near Basilica of San Lorenzo. Settled in the historical city center, the observatory is surrounded by a network of Medieval and Renaissance narrow streets and alleyways. Emissions of airborne pollutants in the city center are mainly related to vehicular traffic and domestic heating (allowed by local government from 5:00 to 23:00 starting from the 1st of November to the 15th of April of each year), whilst additional emission sources are

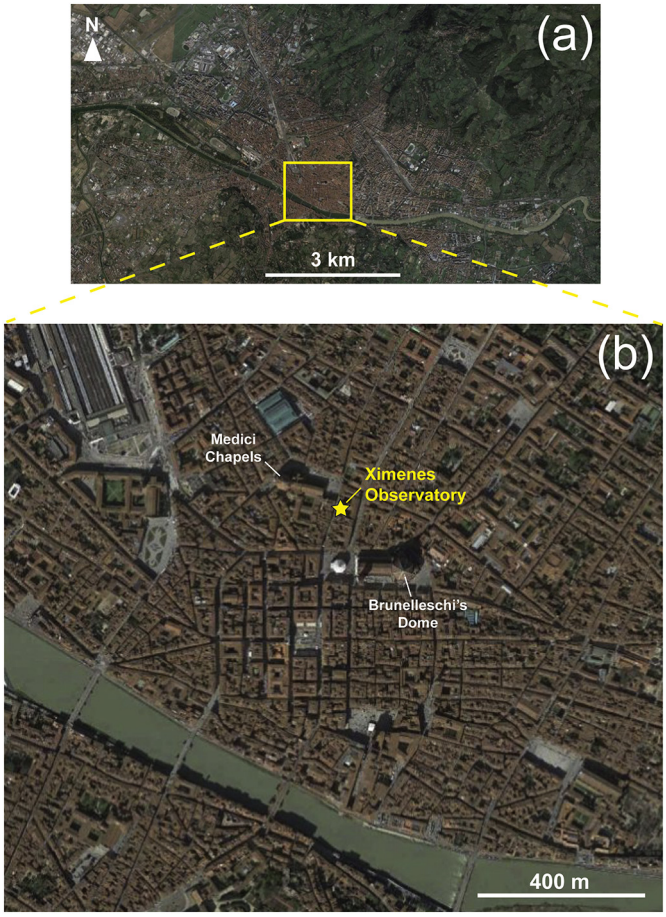

Fig. 1. Satellite image of **(a)** metropolitan area and **(b)** historical center of Florence, where the location of the monitoring site (Ximenes Observatory) is shown (yellow star). (For interpretation of the references to colour in this figure legend, the reader is referred to the web version of this article.)

present in the outskirts of the city, including an international airport, two major highways and light industry districts.

2.2. Rooftop gas monitoring

A reference weather station was installed on the roof of the Ximenes Observatory, equipped with the following sensors: air temperature and humidity (Vaisala HMP155), wind speed and direction (Young wind sentry 03002), solar radiation (Kipp Zonen CMP3 Pyranometer), pluviometer (Delta-T - Model RG1 + BP-06 - Rain gauge) and a data logger (Campbell CR-1000). Data, collected every 10 min, were stored locally on a CR-1000 data logger and transferred to the CNR-IBIMET web server.

Turbulent fluxes of energy, momentum and CO_2 at half-hourly intervals were measured with the eddy covariance technique (e.g. Grimmond et al., 2002; Matese et al., 2009; Gioli et al., 2012; Vaccari et al., 2013). A 7 m long mast was erected above the roof level. The eddy covariance setup consisted of sonic anemometer 3 axes (Metek USA-1), fast IRGA open path CO_2 and H_2O gas analyzer (Licor LI-7500A). The raw data were collected at the frequency of 20 Hz. Quality-control procedures included despiking, instrument failure detection in rainy conditions, and stationarity analysis (Foken and Wichura, 1996). Single point storage correction was applied as described in Papale et al. (2006). A threshold friction velocity equal to 0.13 m/s was derived by analyzing the dependence of nighttime CO_2 flux on $u*$ on selected periods and detecting the value beyond which the flux levelled off. The storage correction was applied before the $u*$ correction to avoid the double counting effect. Data that failed quality criteria were gap-filled with a procedure based on a mean diurnal variation (Falge et al., 2001), where a missing observation at a certain time was replaced by the mean for that time based on adjacent days. A number of 10 adjacent days was used. Path averaging and sensor separation corrections were applied using the Moore (1986) first order transfer functions. A footprint analysis was made based on the analytical model described in (Hsieh et al., 2000). The upwind distances containing 50% and 90% of measured flux were computed as a function of wind speed and direction, atmospheric stability, measurement height and surface roughness, and resulted to be 445 m and 1070 m, on average, respectively. Roughness length for this site was previously calculated (Gioli et al., 2015) using a regression-based fitting of the universal function in the logarithmic wind profile as described in Graf et al. (2014), and resulted in the 0.3–0.6 m range depending on the wind sector.

The concentrations and $\delta^{13}C$ values (expressed in ppm and ‰ vs. V-PDB, respectively) of CO_2 and CH_4 in air were monitored using a WS-CRDS (Wavelength-Scanned Cavity Ring Down Spectroscopy) – based analyzer (Picarro G2201-i) housed within a storage room on the roof the Ximenes Observatory. Air samples were drawn from a window through Teflon tubing using a vacuum pump (sampling rate: 25 mL min^{-1}). The instrument was operated nearly continuously from the 7th to the 21st of July 2017 and from the 10th of October to the 15th of December 2017. Calibration was performed at the beginning of the two measuring periods using the following standards (Air Liquide): (i) 380, 500 and 1000 ppm CO_2, (ii) 1.8, 5 and 10 ppm CH_4, (iii) −44, −5 and +2‰ $\delta^{13}C$-CO_2, and (iv) -60 and −25‰ $\delta^{13}C$-CH_4 (Air Liquide). The precision was within 0.2 ppm CO_2, 0.05 ppm CH_4, 0.16‰ $\delta^{13}C$-CO_2 and 1.15‰ $\delta^{13}C$-CH_4. The instrument was further checked once a month using the above-mentioned standards. Half-hourly averages were obtained from the dataset acquired from each instrument and used for further data processing. Data reduction (monthly, daily and hourly averages) and analysis were performed using R (R Core Team, 2017) implemented with the Openair package (Carslaw and Ropkins, 2012; Carslaw, 2014). The acquired data were referred to local time, i.e. (i) CEST (Central European Summer Time) from the 7th of July to the 29th of October 2017 and (ii) CET (Central European Time) from the 29th of October to the 15th of December 2017.

3. Results

3.1. Meteorological parameters

The temperature showed a relevant seasonal variation, with monthly average values of 26.9, 15.5, 10.5 and 8.1 °C in July, October, November and December, respectively. The diurnal changes in temperature were, on average, of 11.3, 12.1, 7.1 and 6.5 °C, respectively, monthly varying from 16.8 to 36.8 °C in July, from 5.3 to 29.1 °C in October, from −0.3 to 19.3 °C in November and from −0.7 to 16.6 °C in December. The minimum hourly-average temperature was recorded in early morning (from 5:00 to 8:00), whereas the maximum value was observed in early afternoon (from 15:00 to 16:00) (Fig. 2).

The monthly-average relative humidity was relatively low in July (37%) and increased during fall with values of 59, 68 and 67% in October, November and December, respectively. Accordingly, no meteoric events were recorded in July 2017, when Italy was facing a drought emergency, whilst rainfall occurred in 2, 13 and 9 days in October, November and December 2017, respectively, with precipitation values that did not exceed 4.8, 14.6 and 5.6 mm per day, respectively.

Average wind speed was 2.51, 1.38, 1.60 and 2.10 m/s in July, October, November and December, respectively, in agreement with the average value (2.52 m/s) recorded from 1993 to 2010 by Gualtieri et al. (2014), indicating the occurrence of relatively poor advection conditions. Prevailing winds blew from SE (Fig. 3), followed by (i) W, NE and WNW in July, (ii) WNW, ESE and SSE in October, (iii) NE, SSE and

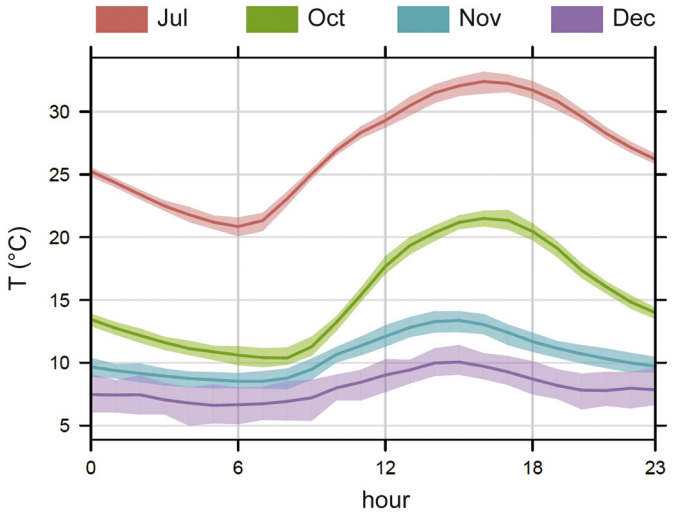

Fig. 2. Diurnal variations in temperature for each month. The bold line shows hourly means, whilst the shaded areas represent 95% confidence intervals.

ENE in November and (iv) SSW, SSE and SW in December. Maximum wind speed values were associated with winds blowing from NE (7.57 m/s), W (6.21 m/s), NE (7.75 m/s) and SW (8.17 m/s) in July, October, November and December, respectively.

3.2. Seasonal variations in fluxes, concentrations and $\delta^{13}C$ values of atmospheric CO_2

The half-hourly CO_2 flux ranged from −217 to 3074 μg m^{-2} s^{-1} during the observation period, with an average value of 729 ± 615 μg m^{-2} s^{-1}. The lowest values were measured in July, being from −217 to 2584 μg m^{-2} s^{-1}, whereas higher fluxes were recorded in October and November, i.e. from −216 to 2713 μg m^{-2} s^{-1} and from −213 to 3074 μg m^{-2} s^{-1}, respectively (Fig. 4a). The average CO_2 flux values in July, October and November were 507 ± 400 μg m^{-2} s^{-1}, 636 ± 518 μg m^{-2} s^{-1} and 922 ± 716 μg m^{-2} s^{-1}, respectively.

The CO_2 concentrations and $\delta^{13}C$ values showed similar seasonal fluctuations (Fig. 4b). The CO_2 concentrations were high during the fall season and low in summer, ranging from 395 to 782 ppm with an average value of 450 ± 37.8 ppm. During July, October, November and December, the CO_2 concentrations ranged from 395 to 446 ppm, from 411 to 782 ppm, from 413 to 669 ppm and from 411 to 636 ppm, respectively, with monthly average values of 413 ± 11.9 ppm, 454 ± 34.5 ppm, 460 ± 37.8 ppm and 457 ± 37.6 ppm, respectively. The monthly CO_2 amplitudes were large in October (371 ppm), followed by November and December (256 and 224 ppm, respectively). The lowest amplitude was recorded in July (51 ppm).

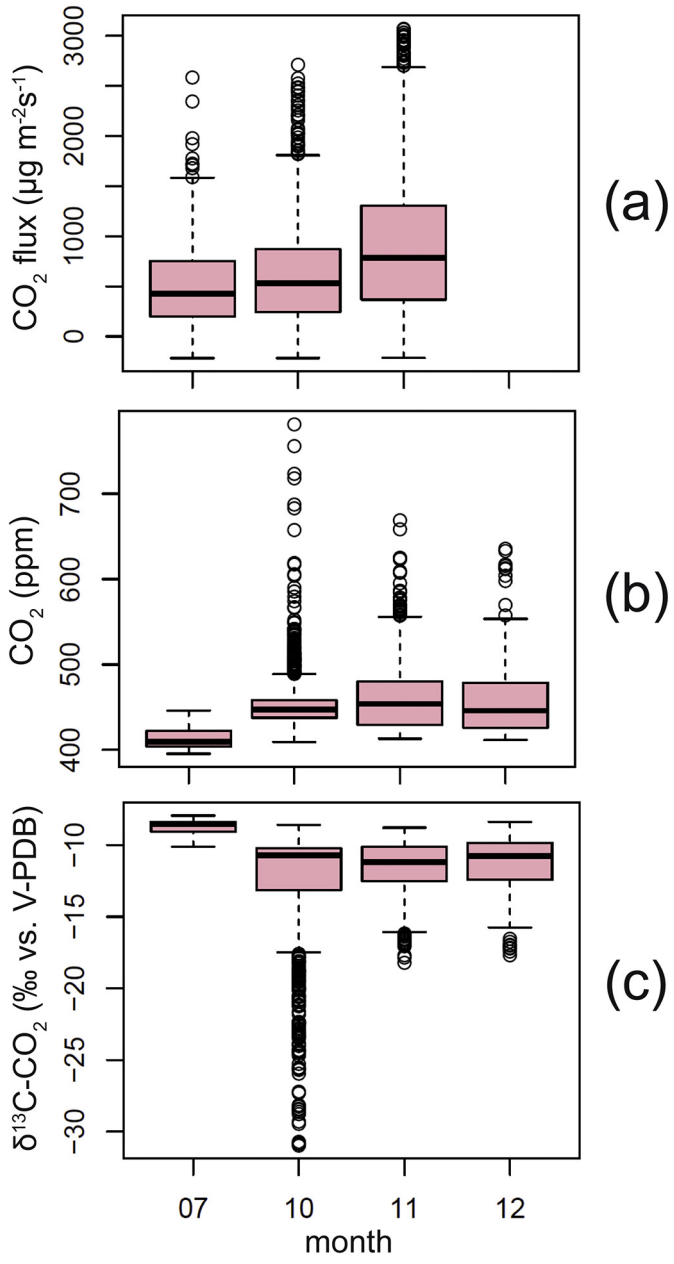

Fig. 4. Boxplots of **(a)** CO_2 fluxes, **(b)** CO_2 concentrations, and **(c)** $\delta^{13}C$-CO_2 values for each month. The median is also shown (black line).

The $\delta^{13}C$ values were inversely correlated to the CO_2 concentrations (Fig. 4c), showing the highest values in July, ranging from −10.1 to

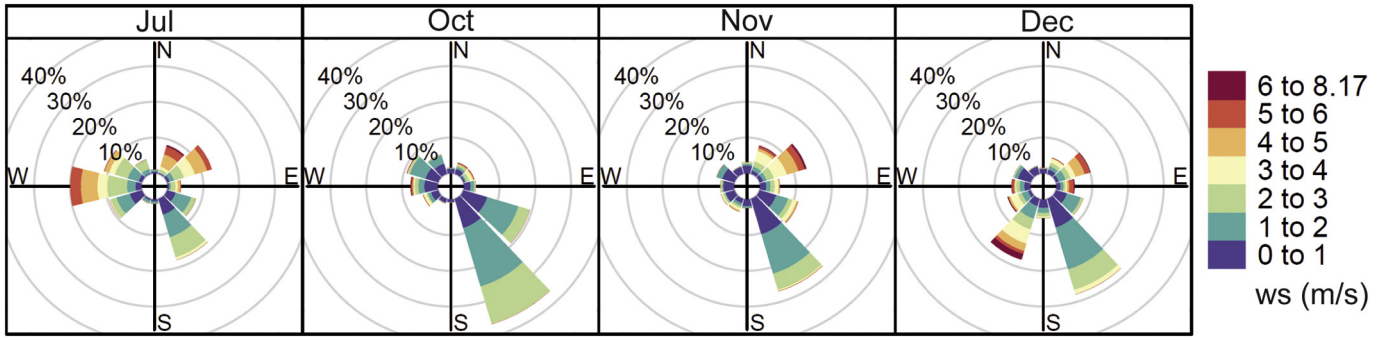

Fig. 3. Wind roses showing wind speed (in m/s) and direction frequencies at the monitoring site referred to each month.

−7.95‰ vs. V-PDB (average value: −8.72 ± 0.47‰ vs. V-PDB), and the lowest values during fall, ranging from −31.0 to −9.10‰ vs. V-PDB, from −18.2 to −8.79‰ vs. V-PDB and from −17.7 to −8.38‰ vs. V-PDB in October, November and December (average values: −12.4 ± 3.82‰ vs. V-PDB, −11.5 ± 1.73‰ vs. V-PDB, −11.2 ± 1.82‰ vs. V-PDB, respectively). The monthly $\delta^{13}C$ amplitudes were relatively large in October (22‰ vs. V-PDB), followed by November and December (9.41 and 9.31‰ vs. V-PDB, respectively), and low in July (2.17‰ vs. V-PDB).

3.3. Diurnal variations in fluxes, concentrations and $\delta^{13}C$ values of atmospheric CO_2

The CO_2 flux showed a clear, and relatively constant, diurnal cycle during the observation period (Fig. 5a). The lowest CO_2 flux values were measured during nighttime and early morning, in particular from 02:00 to 07:00 in July, from 02:00 to 06:00 in October and from 01:00 to 05:00 in November, with average daily amplitudes of 174 ± 30.4 μg m^{-2} s^{-1}, 216 ± 25.9 μg m^{-2} s^{-1}, and 341 ± 10.6 μg m^{-2} s^{-1}, respectively. The CO_2 fluxes were then rapidly increasing up to a peak value of 836 μg m^{-2} s^{-1} at 13:00 in July 1022 μg m^{-2} s^{-1} at 12:00 in October and 1333 μg m^{-2} s^{-1} at 08:00 in November. The CO_2 emissions then progressively decreased down to 635 μg m^{-2} s^{-1} at 17:00 in July, 657 μg m^{-2} s^{-1} at 21:00 in October and 945 μg m^{-2} s^{-1} at 16:00 in November and afterwards a second peak value was recorded at 23:00 in July, at 22:00 in October and at 21:00 in November, with values of 806, 998 and 1421 μg m^{-2} s^{-1}, respectively.

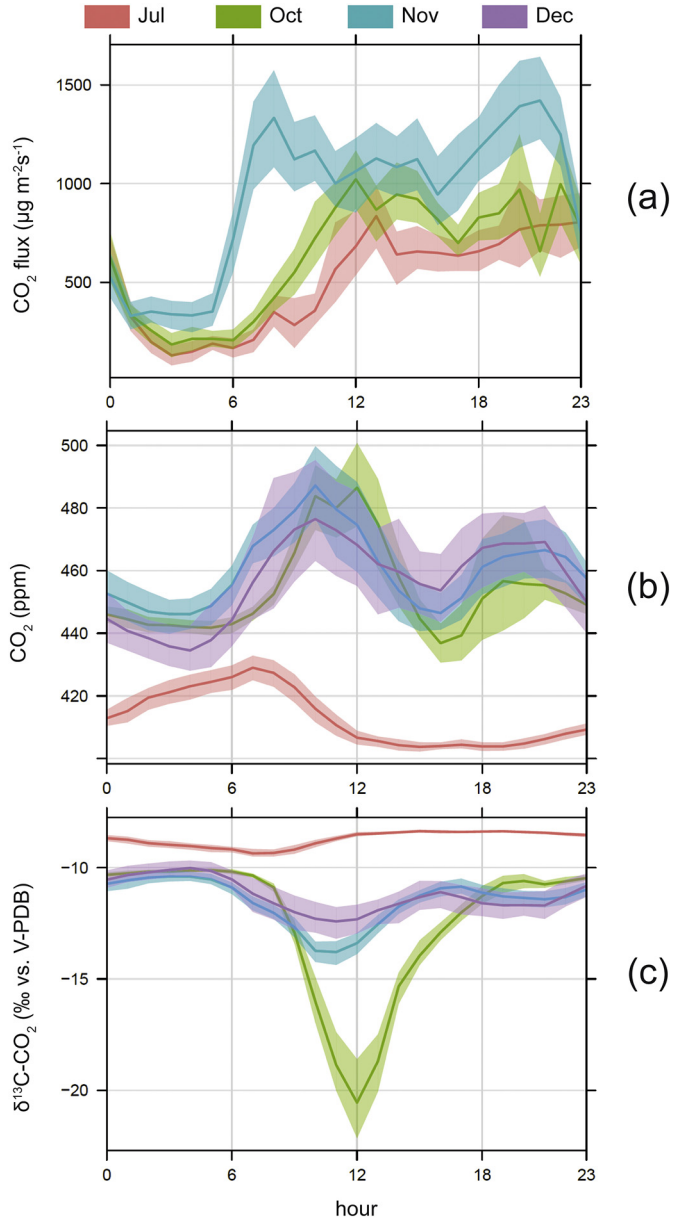

Fig. 5. Diurnal variations of **(a)** CO_2 fluxes, **(b)** CO_2 concentrations, and **(c)** $\delta^{13}C$-CO_2 values for each month. The bold line shows hourly mean values, whilst the shaded areas represent 95% confidence intervals.

The hourly mean CO_2 concentrations and $\delta^{13}C$ values are shown in Fig. 5b,c. Whilst the diurnal cycle of CO_2 concentrations was similar to that of the CO_2 flux during the fall season, an opposite trend was observed in summer (Fig. 5a,b). Interestingly, in July, the highest CO_2 concentrations were measured during nighttime and early morning with a progressive increase starting from 22:00 and reaching a peak value of 429 ppm at 7:00. On the other hand, the CO_2 concentrations were constantly low (from 404 to 406 ppm) from 13:00 to 21:00. Contrarily, during fall, low CO_2 concentrations were observed from 02:00 to 06:00 in October (from 442 to 443 ppm), from 01:00 to 05:00 in November (from 446 to 450 ppm) and from 00:00 to 06:00 in December (from 434 to 445 ppm). A two-peaks diurnal cycle was observed during fall. The first peak occurred at 12:00 in October and at 10:00 in November and December, with values of 486, 487 and 476 ppm, respectively. The second peak was observed at 19:00 in October, at 21:00 in November and December, with values of 457, 467 and 469 ppm, respectively. The two peaks were interspersed with a phase of decreased CO_2 concentrations down to 437, 446 and 454 ppm at 16:00 in October, November and December, respectively.

The $\delta^{13}C$ values were inversely correlated to the CO_2 concentrations (Fig. 5b,c). The highest $\delta^{13}C$ values were measured during low CO_2 concentration periods, i.e. from 13:00 to 21:00 in July, from 02:00 to 06:00 in October, from 01:00 to 05:00 in November and from 00:00 to 06:00 in December, with average values of −8.40 ± 0.03‰ vs. V-PDB, −10.20 ± 0.03‰ vs. V-PDB, −10.50 ± 0.08‰ vs. V-PDB, and −10.30 ± 0.21‰ vs. V-PDB, respectively. On the other hand, the lowest $\delta^{13}C$ values occurred almost concomitantly with the highest CO_2 concentrations, i.e. at 07:00 in July, at 12:00 in October and at 11:00 in November and December, with values of −9.36, −20.6, −13.8 and −12.4‰ vs. V-PDB, respectively.

3.4. Seasonal variations in the concentrations and $\delta^{13}C$ values of atmospheric CH_4

During the observation period, the CH_4 concentrations ranged from 1.87 to 3.21 ppm, with an average value of 2.23 ± 0.23 ppm. As shown in Fig. 6a, the lowest values were recorded in July (from 1.87 to 2.72 ppm; monthly average: 2.00 ± 0.09 ppm). Similar values were measured in December (from 1.95 to 2.88 ppm; monthly average: 2.17 ± 0.17 ppm), whilst the highest values were measured in October (from 1.98 to 3.16 ppm; monthly average: 2.39 ± 0.22 ppm) and November (from 1.99 to 3.21 ppm; monthly average: 2.25 ± 0.20 ppm).

The $\delta^{13}C$-CH_4 values showed dramatic seasonal variations (Fig. 6b). In July, the lowest $\delta^{13}C$-CH_4 values were recorded, ranging from −54.0 to −46.7‰ vs. V-PDB, with a monthly average value of −51.1 ± 1.7‰ vs. V-PDB. Significantly higher values were measured during the fall season, ranging from −51.7 to −43‰ vs. V-PDB in October (monthly average: −44.8 ± 0.8‰ vs. V-PDB), from −47.5 to −43.5‰ vs. V-PDB in November (monthly average: −44.9 ± 0.4‰ vs. V-PDB), and from −46.1 to −43.6‰ vs. V-PDB in December (monthly average: −45.1 ± 0.4‰ vs. V-PDB).

3.5. Diurnal variations in the concentrations and $\delta^{13}C$ values of atmospheric CH_4

The hourly average CH_4 concentrations and $\delta^{13}C$ values are shown in Fig. 7. The diurnal cycle of the CH_4 concentrations (Fig. 7a) was similar

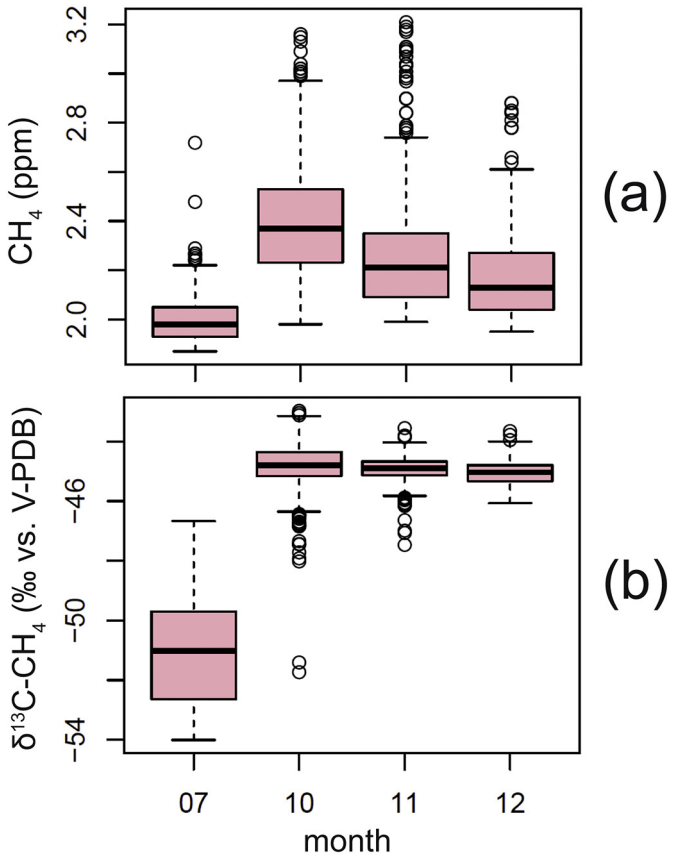

Fig. 6. Boxplots of **(a)** CH_4 concentrations, and **(b)** $\delta^{13}C$-CH_4 values for each month.

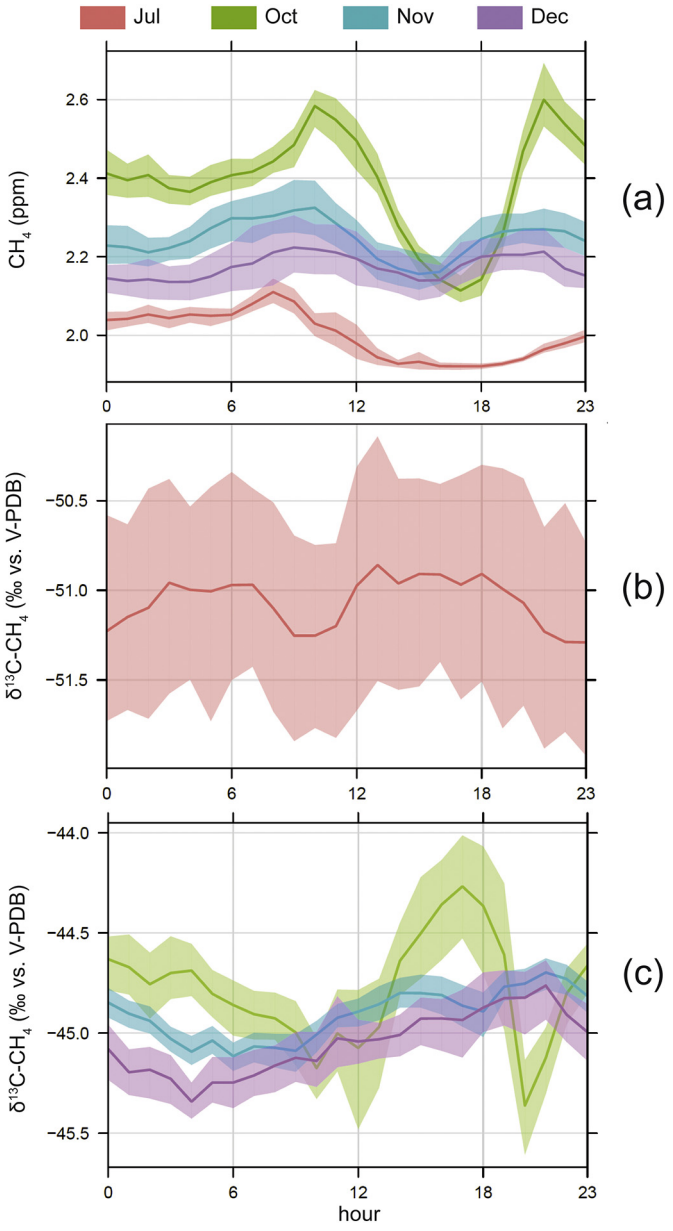

Fig. 7. Diurnal variations of **(a)** CH_4 concentrations, and **(b)** $\delta^{13}C$-CH_4 values for each month. The bold line shows hourly mean values, whilst the shaded areas represent 95% confidence intervals.

to that of CO_2 (Fig. 5b). In July, the highest CH_4 concentrations were measured during nighttime, with values gradually increasing from 19:00 to a peak value of 2.11 ppm at 8:00, whereas the lowest hourly average CH_4 concentrations (1.92 ppm) were recorded from 16:00 to 18:00. During fall, two peaks were recognized. The first one occurred from 9:00 to 10:00 with values up to 2.58, 2.32 and 2.22 ppm in October, November and December, respectively. The second one was detected at 21:00 with values up to 2.60, 2.27 and 2.21 ppm in October, November and December, respectively. The two peaks were interspersed with a phase of low CH_4 concentrations between 15:00 and 17:00, with CH_4 concentrations down to (i) values (down to 2.16 and 2.14 ppm, respectively) comparable to those recorded during nighttime (down to 2.21 and 2.14 ppm, respectively) in November and December, and (ii) values (down to 2.11 ppm) markedly lower than those recorded during nighttime (down to 2.37 ppm) in October.

The hourly average $\delta^{13}C$ values varied in a narrow range, i.e. 0.4‰ vs. V-PDB in July and December (i.e. from −51.3 to −50.9‰ vs. V-PDB and from −45.3 to −44.8‰ vs. V-PDB, respectively), 0.6‰ vs. V-PDB in November (i.e. from −45.1 to −44.7‰ vs. V-PDB) and 1.1‰ vs. V-PDB in October (i.e. from −45.4 to −44.3‰ vs. V-PDB). In November and December, the diurnal cycle of $\delta^{13}C$ values was comparable, with lowest values at night (around 3:00) followed by a progressive increase during daytime until 21:00. A different pattern was observed in October, when a peak in $\delta^{13}C$, up to −44.3‰ vs. V-PDB, was observed at 17:00, followed by a decrease down to a minimum value of −45.4‰ vs. V-PDB at 20:00.

4. Discussion

4.1. Urban CO_2 footprint

Due to both local morphology and meteorological conditions (the hills bordering the alluvial plain affect atmospheric circulation limiting the dispersion of air pollutants), the urban area of Florence is particularly prone to the accumulation and trapping of air contaminants in the lower atmosphere leading to poor air quality conditions (Gualtieri et al., 2014), especially during the cold season.

According to our data, monthly average CO_2 fluxes from the city measured in October and November were 26% and 82% higher than those observed in July, respectively. The constant diurnal cycle of CO_2 fluxes over summer and fall seasons characterized by highest values from the sunrise until few hours after the sunset indicates that the CO_2 emissions were strictly related to anthropogenic sources. Although negative values were occasionally measured (corresponding to 4, 5 and 2% of data in July, October and November, respectively), the CO_2 fluxes from the city were mostly positive during the entire observation period. This indicates that the metropolitan site acts as a net source of CO_2 and that the current urban green infrastructures (including urban forests, ~10% of the total city area; Bottalico et al., 2016, 2017) are not sufficient to counterbalance the emissions from anthropogenic activities even during the plant vegetative period, as observed in other mid-latitude

cities (e.g. Velasco et al., 2005, 2009; Velasco and Roth, 2010 and references therein).

In July, the diurnal cycle of the CO_2 concentrations clearly reflected the evolution of the atmospheric boundary layer (Fig. 5b). During nighttime, gas accumulation occurred due to the stable atmospheric conditions characterizing the nocturnal boundary layer (NBL). After sunrise, heating of the surface drives the establishment of the turbulent convective boundary layer (CBL) that favors dispersion and dilution of the air contaminants. On the other hand, during the fall season, the dilution effect induced by the onset of the CBL was completely overwhelmed by the diurnal CO_2 emissions from the urban area.

4.1.1. CO_2 sources

The emitting sources responsible for CO_2 discharges into the atmosphere from the urban area of Florence were investigated on the basis of the Keeling plot analysis. The method derives from a simple two end-member mixing model between background and local source(s), based on the following mass balance equations:

$$C_m = C_b + C_s \quad (1)$$

$$\delta^{13}C_m \times C_m = \delta^{13}C_b \times C_b + \delta^{13}C_s \times C_s \quad (2)$$

where C and $\delta^{13}C$ are the concentration and the carbon isotopic composition of the gas species, respectively, and m, b and s subscripts refer to the measured, background and source(s) values, respectively.

These equations can be arranged in the following form:

$$\delta^{13}C_m = \frac{\left(\delta^{13}C_b - \delta^{13}C_s\right) \times C_b}{C_m} + \delta^{13}C_s \quad (3)$$

Eq. (3) identifies a straight line on a $1/C$ vs. $\delta^{13}C$ plot whose intercept corresponds to the isotopic signature of the emitting source. According to this approach, first proposed by Keeling (1958, 1961), the background values can remain unknown, but both the background and source(s) values have to be constant during the observation period (Pataki et al., 2003a, 2003b).

In Fig. 8a, only nighttime data (h 0–5) were used to construct Keeling plots, since (i) stable weather conditions allow the locally emitted CO_2 to be accumulated in the atmosphere, (ii) photosynthesis effects can be ignored, and (iii) active anthropogenic emissions are minimal. Consequently, a weighted average isotopic value of the daily emitted CO_2 from multiple sources can be derived. Summer data plot along the mixing line of global background CO_2 (407 ppm with $\delta^{13}C$ value of −8.6‰ vs. V-PDB, as annual average measured in 2017 at

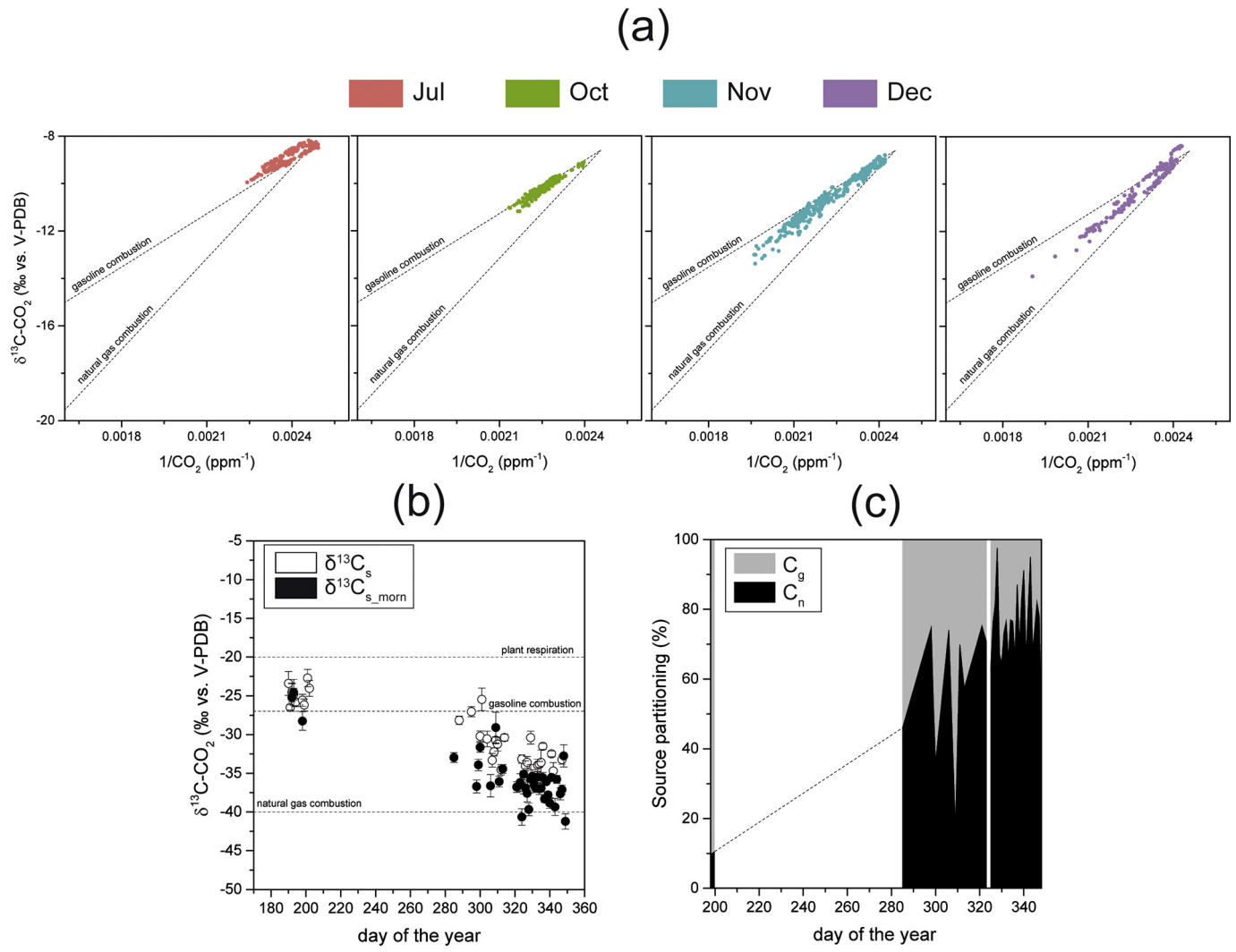

Fig. 8. (a) Keeling plots of $\delta^{13}C$-CO_2 vs. $1/CO_2$ for each month referred to nighttime data (h 0–5). The dashed lines show mixing between the background values and either gasoline (upper line) or natural gas (lower line) combustion. **(b)** Estimated $\delta^{13}C_s$ (white circles) and $\delta^{13}C_{s\_morn}$ (black circles) values during the monitoring period (see text for details). The dashed lines show $\delta^{13}C$-CO_2 values related to plant respiration, gasoline combustion and natural gas combustion. **(c)** Relative contribution of gasoline (grey field) and natural gas (black field) combustion to atmospheric CO_2 (see text for details).

Mauna Loa Observatory; Keeling et al., 2005) with CO_2 produced by gasoline combustion (mainly related to road traffic: ca. −27‰ vs. V-PDB; Clark-Thorne and Yapp, 2003; Zimnoch, 2009; Górka and Lewicka-Szczebak, 2013 and references therein; Chamberlain et al., 2016), with some data plotting above the mixing line due to possible contributions from C3 plant respiration (from −26.5 to −20‰ vs. V-PDB; Górka and Lewicka-Szczebak, 2013 and references therein). Fall data plot below the gasoline line, progressively approaching the mixing line with natural gas combustion (ca. −40‰ vs. V-PDB; Clark-Thorne and Yapp, 2003; Górka and Lewicka-Szczebak, 2013; Chamberlain et al., 2016) from October to December. A data filtering was operated in order to ensure reliable $\delta^{13}C_s$ estimates, according to the following criteria: (i) a sufficient CO_2 concentration range (≥15 ppm; Zobitz et al., 2006) was measured each night; (ii) linearity in the OLS regression of $\delta^{13}CO_2$ on $1/CO_2$ was checked applying significance and r^2 thresholds ($P < 0.05$ and $r^2 > 0.75$; Chamberlain et al., 2016); and (iii) the intercept standard errors were lower than 2‰ (Chamberlain et al., 2016 and references therein). Overall, after applying the quality control criteria, about 40% of data remained. The estimated $\delta^{13}C_s$ values of the emitted CO_2 ranged from −26.5 to −22.7‰ vs. V-PDB in July, from −30.6 to −25.5‰ vs. V-PDB in October, from −36.4 to −30.4‰ vs. V-PDB in November and from −34.7 to −31.5‰ vs. V-PDB in December, confirming the increased contribution from natural gas combustion in the colder season (Fig. 8b). The same procedure was adopted to calculate the $\delta^{13}C_s$ values ($\delta^{13}C_{s\_morn}$) from data measured in early morning (i.e. h 5–9 in July, h 6–8 in October, h 5–8 in November; for December, the time interval used for November was selected), when the CO_2 fluxes showed a sharp increase. The $\delta^{13}C_{s\_morn}$ values more strictly represent the isotopic signature of the anthropogenic sources actively contributing to CO_2 emissions during daytime. The resulting values (from −28.3 to −24.6‰ vs. V-PDB in July, from −36.7 to −31.7‰ vs. V-PDB in October, from −40.6 to −29.1‰ vs. V-PDB in November and from −41.2 to −32.8‰ vs. V-PDB in December) were slightly more negative than those obtained in nighttime (Fig. 8b). Under the dim light conditions of the early morning, photosynthetic uptake is expected to match the rate of cellular respiration, so that CO_2 is neither produced nor consumed by the biosphere. Accordingly, the $^{13}C_{s\_morn}$ values were to be considered as the result of time-varying contributions to atmospheric CO_2 from gasoline and natural gas combustion, according to the following mass balance equations:

$$C_s = C_g + C_n \tag{4}$$

$$\delta^{13}C_s \times C_s = \delta^{13}C_g \times C_g + \delta^{13}C_n \times C_n \tag{5}$$

where *g* and *n* subscripts refer to gasoline and natural gas combustion, respectively, and other symbols were as in Eqs. (1) and (2). Accordingly, the relative contribution of the two sources can be derived, as follows:

$$\frac{C_n}{C_s}(\%) = 100 \times \frac{\delta^{13}C_s - \delta^{13}C_g}{\delta^{13}C_n - \delta^{13}C_g} \tag{6}$$

$$\frac{C_g}{C_s}(\%) = 100 - \frac{C_n}{C_s} \tag{7}$$

According to our estimation, gasoline and natural gas combustion accounted for about 32 and 68% of non-background atmospheric CO_2 during the whole observation period (Fig. 8c), respectively, in good agreement with previous estimations (Gioli et al., 2012, 2015). The estimated C_g values were high in July (about 90%), whereas those of C_n progressively increased during fall up to ~75% in December (Fig. 8c). Since the vehicular traffic has no relevant seasonal changes in Florence (Matese et al., 2009; Gioli et al., 2012), the variations in the C_n/C_g ratios were entirely ascribed to different contributions of CO_2 emissions from natural gas combustion. In December, the latter appeared to be 7 times higher than in July, an estimation in agreement with the increasing use of natural gas (ca. 10% in summer and ca. 70% in winter; Matese et al., 2009).

4.1.2. CO_2 sinks

During daytime, both (i) dilution and dispersion due to either air mass convection or wind transport, and (ii) photosynthetic uptake may contribute to partially offset the increase in atmospheric CO_2 concentrations due to anthropogenic emissions. In terms of isotopic effects, these two processes are expected to produce different outcomes. Dilution and dispersion isotopically consist in a mixing process between local and background air. Conversely, photosynthetic uptake of atmospheric CO_2 results in C isotope fractionation, as plants preferentially assimilate $^{12}CO_2$ (e.g. Lloyd and Farquhar, 1994).

As evidenced in Fig. 9, in daytime (h 6–18), when the $\delta^{13}C$-CO_2 values are plotted versus $1/CO_2$ ratios, some data are not consistent with simple dilution and dispersion phenomena, being characterized by $\delta^{13}C$-CO_2 values lower than those expected for mixing between background air and emitting sources. Negative shifts of $\delta^{13}C$-CO_2 values >2‰ vs. V-PDB were recorded from 9:00 to 17:00 in October and from 9:00 to 13:00 in November. Although these negative shifts of $\delta^{13}C$-CO_2 were observed in days characterized by prevailing winds blowing from the NW sector rather than SE, the largest drifts (>5‰ vs. V-PDB) were associated with wind speeds <2 m/s, indicating that contributions from distal sources were unlikely while a low dispersion of locally emitted CO_2 was expected. At this regard, it is worth noting that the maximum isotopic shifts were measured in the central hours of the day, i.e. at 12:00 in October and at 11:00 in November, when the maximal photosynthetic uptake was expected to occur. According to Vaccari et al. (2013), the green spaces (29.1 km^2) within the Municipality of Florence (102.3 km^2) would offset ~6% of direct carbon emissions.

The isotopic effect of photosynthetic uptake can be modelled through a Rayleigh-type equation:

$$\delta^{13}CO_{2\_res} = \left(1000 + \delta^{13}CO_{2\_ini}\right) f^{\left(\frac{1}{\alpha_{air\_plant}} - 1\right)} - 1000 \tag{8}$$

where f is the fraction of residual CO_2 in the atmosphere, $\delta^{13}CO_{2\_res}$ and $\delta^{13}CO_{2\_ini}$ are the isotopic composition of CO_2 before and after the photosynthetic removal, respectively, and α_{air_plant} (1.0183; Lloyd and Farquhar, 1994) is the isotopic fractionation factor during the photosynthetic withdrawal. As evidenced by the calculated trajectory for the evolution of $1/CO_2$ and $\delta^{13}C$-CO_2 shown in Fig. 9, the photosynthetic removal of atmospheric CO_2, characterized by different and continually changing initial values during daytime, might explain the shift of isotopic data below the mixing line between background air and anthropogenic sources. A similar effect was observed by Clark-Thorne and Yapp (2003) in the metropolitan area of Dallas (USA). The relevance of the impact of photosynthetic activity on the measured data showed a sharp seasonality, because of both (i) seasonal cycles of plants in response to changes in temperature, humidity and irradiance conditions and (ii) waxing and waning of anthropogenic emissions. In July, photosynthetic uptake had virtually no substantial impact. According to Vaccari et al. (2013), urban green spaces in Florence were at their lowest CO_2 offset capacity during mid-summer, due to the dry conditions typically characterizing the Mediterranean ecosystems. Moreover, according to the Institute of Atmospheric Sciences and Climate (CNR-ISAC), 2017 was the Italy's driest year of the last two centuries. On the other hand, the progressive increase in anthropogenic CO_2 emissions during fall (Fig. 4a) was likely overwhelming the photosynthetic removal, which was further hindered by the low temperatures (Fig. 2). Accordingly, the maximum shifts of $\delta^{13}C$-CO_2 values were observed concomitantly with the first diurnal peak of CO_2 concentrations (Fig. 5b), indicating a concurrence of maximal photosynthetic removal with anthropogenic emissions climax. Ultimately, the sharpest influence of photosynthetic activity on atmospheric $\delta^{13}C$-CO_2 values was observed

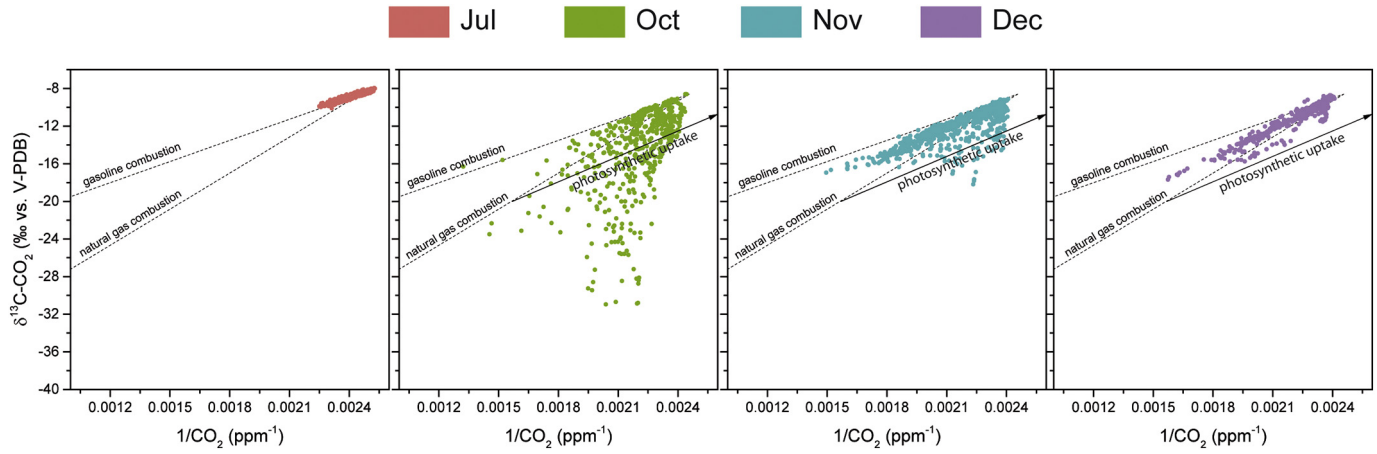

Fig. 9. Keeling plots of δ^{13}C-CO_2 vs. 1/CO_2 for each month referred to daytime data (h 6–18). The dashed lines show mixing between the background values and either gasoline (upper line) or natural gas (lower line) combustion. The black arrow shows the isotopic effect related to photosynthetic uptake of atmospheric CO_2.

in October, when the temperature was still relatively mild and housing heating was still restricted. To verify the hypothesis about the role of photosynthetic activity with independent observations, we analyzed the vegetative status of the study area with monthly MODIS satellite NDVI, selected as a proxy for photosynthetic activity. Although NDVI is a vegetation index, therefore not directly linked to actual photosynthetic rate but rather to canopy chlorophyll content, together with fAPAR (fraction of absorbed photosynthetically active radiation), it is widely considered a robust proxy for estimating Net Primary Productivity (NPP) of vegetation at coarse temporal resolution (Running et al., 2004). Monthly NDVI data (Fig. 10) confirmed the typical pattern of Mediterranean ecosystems since they experience a strong spring vegetative strength, a summer drought associated with low NDVI, and a fall recovery that may peak in September to November, depending on climate conditions. In 2017, October and November were indeed the months with the largest NDVI value among the sampled months, supporting the hypothesis that observed negative shifts of δ^{13}C-CO_2 (Fig. 9) were likely driven by plant photosynthesis at the regional scale, considering the Florence peri-urban green areas.

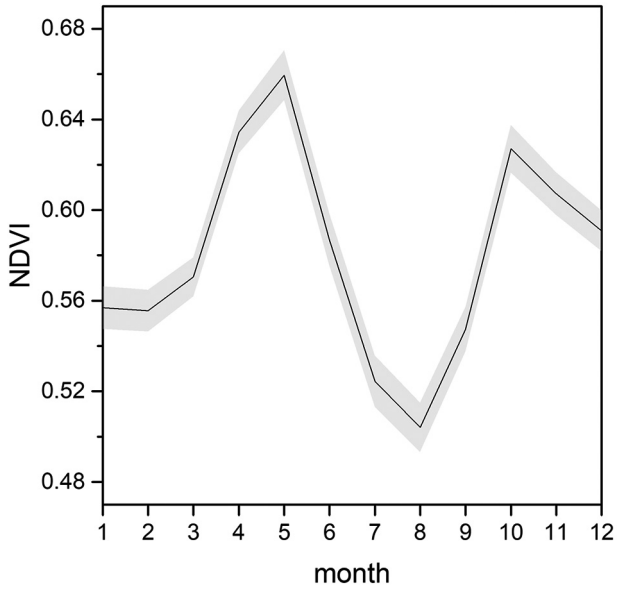

Fig. 10. NDVI data obtained from the MOD13A3 product (https://lpdaac.usgs.gov/dataset_discovery/modis/modis_products_table/mod13a3_v006), distributed at monthly temporal resolution and 1 km spatial resolution. Mean values of an area of 25 × 25 km centered on the measurement site were computed, with the corresponding 95% confidence intervals. Grid cells with an NDVI value lower than 0.2, likely related to entirely urban surfaces, were excluded from the computation.

4.2. Urban CH_4 levels and emitting sources

The measured CH_4 concentrations constantly exceeded the global background value (~1.85 ppm in 2017; Dlugokencky, 2018; Fig. 6a), as commonly observed in urban areas (e.g. Lowry et al., 2001; Nakagawa et al., 2005; Górka et al., 2014; Chamberlain et al., 2016; Zazzeri et al., 2017) and, in general, they were inversely correlated to wind speeds, suggesting that CH_4 levels in air were mostly related to boundary layer dynamics and local sources. Seasonal fluctuations in CH_4 concentrations in air were observed (Fig. 6a), the monthly average values measured in October, November and December being 8.5, 20 and 13% higher than those observed in July, respectively. Similarly, a sharp excursion in the isotopic data towards heavier values was observed in fall with respect to summer (Fig. 6b). The observed seasonal trends in both concentrations and CH_4 isotopic ratios point to the occurrence of variations in relative contributions from emitting sources and active sinks during the year.

The diurnal cycle of CH_4 concentrations (Fig. 7a) was relatively similar to that observed for those of CO_2, suggesting the occurrence of common emitting sources for the two gaseous contaminants and/or a strict control of the boundary layer dynamics. On the other hand, the isotopic ratios of CH_4 showed a less clear diurnal variation. In July, the δ^{13}C-CH_4 values were relatively constant (Fig. 7b), pointing to the absence of relevant local emitting sources during daytime, and oscillating around −51‰ vs. V-PDB. This value is similar to those reported for biogenic sources, including landfills (around −58‰ vs. V-PDB; e.g. Zazzeri et al., 2017), agriculture- and livestock-related emissions (from −66 to −55‰ vs. V-PDB; e.g. Levin et al., 1993; Lowry et al., 2001; Townsend-Small et al., 2012; Zazzeri et al., 2017 and references therein), wetlands (around −60‰ vs. V-PDB; e.g. Quay et al., 1988) and, in particular, emissions from wastewater treatments (around −53‰ vs. V-PDB; Zazzeri et al., 2017). The decrease in CH_4 concentrations during daytime with respect to nocturnal values was consistent with the boundary layer diurnal cycle and possibly enhanced by the degradation of tropospheric methane with OH radicals produced by photolysis of ozone in the summer period (e.g. Cicerone and Oremland, 1988; Bréas et al., 2001). During fall, the δ^{13}C-CH_4 values showed a regular trend in November and December, characterized by minimum values during nighttime and a progressive ^{13}C-enrichment during daytime (Fig. 7c), likely related to emissions from domestic heating and evening traffic trapped in the NBL, as observed in other cities (e.g. Zazzeri et al., 2017). Differently, in October, when the highest monthly average CH_4 concentration was measured, the δ^{13}C-CH_4 values

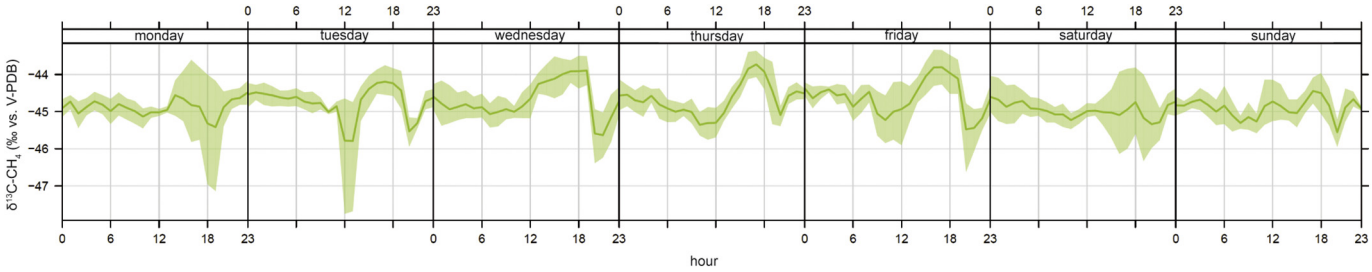

Fig. 11. Weekly variations in δ^{13}C-CH_4 values in October. The bold line shows hourly means, whilst the shaded areas represent 95% confidence intervals.

appeared to be inversely correlated to the diurnal variations of the concentrations, the heavier isotopic ratios being associated with the minimum CH_4 concentrations around 17:00 (Fig. 7a,c). Whilst the decrease of CH_4 concentrations at 17:00 indifferently characterized weekdays and weekends, the sharp increase in the δ^{13}C-CH_4 values was only recorded during weekdays (Fig. 11), strongly supporting that the observed trend was related to anthropogenic activities. The peak in the δ^{13}C-CH_4 values occurred concomitantly with the rise of vehicular traffic during the evening traffic rush hour, whose emissions are typically characterized by ^{13}C-enriched CH_4 with δ^{13}C values ranging from −32 to −26‰ vs. V-PDB, although even higher values (−9 ± 0.3‰ vs. V-PDB) may result from modern vehicles equipped with catalytic converters (Nakagawa et al., 2005 and references therein).

In Fig. 12, the Keeling plot for δ^{13}C-CH_4 and 1/CH_4 values is reported. Whilst summer data appeared largely dispersed, fall data were apparently aligned along a mixing trend between a background value and a CH_4 emitting source. In order to determine the weighted average isotopic value of the daily emitted CH_4 ($\delta^{13}C_s$) during the fall season, only nighttime (h 0–5) data were taken into account and a data filtering was operated, similarly to that applied for the CO_2 measurements, according to the following criteria (Chamberlain et al., 2016 and references therein): (i) a CH_4 concentration range ≥ 0.1 ppm was measured each night; (ii) linearity in the OLS regression of $\delta^{13}CO_2$ on 1/CO_2 was checked applying significance and r^2 thresholds ($P < 0.05$ and $r^2 > 0.50$); and (iii) the intercept standard errors were lower than 2‰. The resulting $\delta^{13}C_s$ values of the emitted CH_4 ranged from −51.2 to −47.0‰ vs. V-PDB in October, from −55.8 to −46.7‰ vs. V-PDB in November and from −52.1 to −39.6‰ vs. V-PDB in December. These values were lower than those related to vehicular emissions and higher than those associated with emissions from agriculture and waste management. On the other hand, the estimated $\delta^{13}C_s$ values approached the isotopic signature of natural gas (around −44‰ vs. V-PDB; Schwietzke et al., 2016; Sherwood et al., 2017). Since no relevant differences were observed in the $\delta^{13}C_s$ values prior and after November 1, 2018, i.e. the beginning of the domestic heating season, our data suggest that significant emissions of CH_4 in the metropolitan area during the fall season were related to leakage from the natural gas pipeline network, which is relatively constant and de-correlated from actual natural gas usage (Gioli et al., 2012).

5. Conclusions

The continuous monitoring of CO_2 fluxes, and atmospheric CO_2 and CH_4 concentrations and carbon isotopic ratios (δ^{13}C-CO_2 and δ^{13}C-CH_4) performed in July 2017 and from October to December 2017 from the roof of the Ximenes Observatory in Florence revealed that the city largely contributed to the atmospheric emission of GHGs. The release of CO_2 from the urban area was higher during fall and related to human activities (vehicular traffic and, more importantly, domestic heating). Despite the ongoing local policies to reduce carbon footprint related to urban mobility, the estimated vehicular emissions accounted for 90% of local CO_2 sources during summer, whereas 75% of CO_2 emissions during fall were related to domestic heating. Overall, natural gas combustion can then be regarded as the major source of the yearly-emitted CO_2 from Florence, in agreement with monitoring surveys conducted in metropolitan areas worldwide (e.g. Clark-Thorne and Yapp, 2003; Górka and Lewicka-Szczebak, 2013; Moore and Jacobson, 2015; Chamberlain et al., 2016; Pang et al., 2016). From a meta-analysis of the urban eddy covariance datasets, natural gas heating makes Florence the second city in terms of absolute CO_2 emissions to the atmosphere after London (Björkegren and Grimmond, 2018). This ranking is also favored by the presence of relatively high building density, high population density including tourism-related short-term visitors, relatively low energy efficiency due to old urban fabric, and low urban green spaces. This set of characteristics makes this site especially suited to isolate the role and atmospheric signature of anthropogenic sources that are not significantly offset by current green urban infrastructures, even though the δ^{13}C-CO_2 data highlighted an isotopic fractionation of

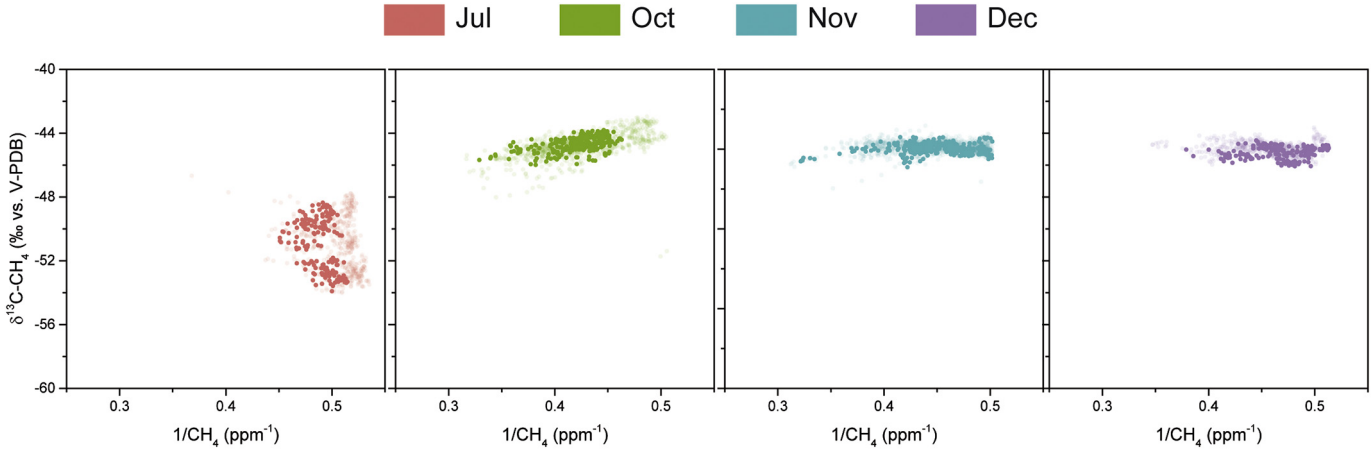

Fig. 12. Keeling plots of δ^{13}C-CH_4 vs. 1/CH_4 for each month referred to nighttime data (h 0–5; solid dots) and daytime data (h 6–23; shaded dots).

atmospheric CO_2 related to photosynthetic activity. Nevertheless, vegetation impacted the CO_2 levels in air for few hours in October and, to a lesser extent, in November, as a consequence of seasonal changes in plant activity related to meteorological parameters, whereas it was overwhelmed by anthropogenic emissions during most of the monitored periods. These results suggest that initiatives directed to reduce anthropogenic CO_2 emitting sources should be complemented by urban planning strategies devoted to massively increase green infrastructures in the metropolitan area.

On the other hand, the seasonal and diurnal trend in concentrations and isotopic composition of CH_4 revealed that the local emitting sources were mainly related to natural gas employment, although vehicular traffic also contributed to the release of this GHG to the atmosphere. Since no relevant changes were observed prior and after the start of the domestic heating, our data suggest that urban CH_4 emissions were mainly related to leakage from the natural gas pipeline network. Similarly, seasonality in urban CH_4 emissions related to natural gas use was reported for other cities, such as Boston (McKain et al., 2015), London (Lowry et al., 2001; Helfter et al., 2016), Łódź (Pawlak and Fortuniak, 2016) and Los Angeles (Townsend-Small et al., 2012), demonstrating that fugitive CH_4 emissions are a major challenge for the assessment of global urban CH_4 budget. Accordingly, in the present study an isotopic partitioning-based top-down approach was applied to provide a valuable alternative for the assessment of fugitive gas emissions to the traditional bottom-up methods, which commonly result in large uncertainties and divergences (e.g. Brandt et al., 2016; Balcombe et al., 2017; Alvarez et al., 2018). Overall, the methodology presented here was successful in partitioning individual contributions to total GHG emissions and proved to be a powerful observational tool to be deployed in cities to improve source categories attributions.

Acknowledgments

The authors wish to thank the Ximenes Observatory foundation for having provided access to the rooftop monitoring site and logistical support. Two anonymous reviewers are greatly acknowledged for their useful comments and suggestions that significantly improved an early version of the manuscript.

References

Alvarez, R.A., Zavala-Araiza, D., Lyon, D.R., Allen, D.T., Barkley, Z.R., Brandt, A.R., Davis, K.J., Herndon, S.C., Jacob, D.J., Karion, A., Kort, E.A., Lamb, B.K., Lauvaux, T., Maasakkers, J.D., Marchese, A.J., Omara, M., Pacala, S.W., Peischl, J., Robinson, A.L., Shepson, P.B., Sweeney, C., Townsens-Small, A., Wofsy, S.C., Hamburg, S.P., 2018. Assessment of methane emissions from the U.S. oil and gas supply chain. Science 361, 186–188. https://doi.org/10.1126/science.aar7204.

ARPAT, 2018. Relazione annuale sullo stato della qualità dell'aria nella regione Toscana anno 2017. ARPAT - Centro regionale tutela qualità dell'aria, p. 123.

Balcombe, P., Anderson, K., Speirs, J., Brandon, N., Hawkes, A., 2017. The natural gas supply chain: the importance of methane and carbon dioxide emissions. ACS Sustain. Chem. Eng. 5, 3–20. https://doi.org/10.1021/acssuschemeng.6b00144.

Björkegren, A., Grimmond, C.S.B., 2018. Net carbon dioxide emissions from central London. Urban Clim. 23, 131–158. https://doi.org/10.1016/j.uclim.2016.10.002.

Bottalico, F., Chirici, G., Giannetti, F., De Marco, A., Nocentini, S., Paoletti, E., Salbitano, F., Sanesi, G., Serenelli, C., Travaglini, D., 2016. Air pollution removal by green infrastructures and urban forests in the city of Florence. Agriculture and Agricultural Science Procedia 8, 243–251. https://doi.org/10.1016/j.aaspro.2016.02.099.

Bottalico, F., Travaglini, D., Chirici, G., Garfì, V., Giannetti, F., De Marco, A., Fares, S., Marchetti, M., Nocentini, S., Paoletti, E., Salbitano, F., Sanesi, G., 2017. A spatially-explicit method to asess the dry deposition of air pollution by urban forests in the city of Florence, Italy. Urban For. Urban Green. 27, 221–234. https://doi.org/10.1016/j.ufug.2017.08.013.

Brandt, A.R., Heath, G.A., Cooley, D., 2016. Methane leaks from natural gas systems follow extreme distributions. Environmental Science & Technology 50, 12512–12520. https://doi.org/10.1021/acs.est.6b04303.

Bréas, O., Guillou, C., Reniero, F., Wada, E., 2001. The global methane cycle: isotopes and mixing ratios, sources and sinks. Isot. Environ. Health Stud. 37 (4), 257–379. https://doi.org/10.1080/10256010108033302.

Carslaw, D.C., 2014. The Openair Manual — Open-Source Tools for Analyzing Air Pollution Data. Manual for Version 1.0. King's College London.

Carslaw, D.C., Ropkins, K., 2012. Openair — an R package for air quality data analysis. Environ. Model Softw. 27-28, 52–61. https://doi.org/10.1016/j.envsoft.2011.09.008.

Chamberlain, S.D., Ingraffea, A.R., Sparks, J.P., 2016. Sourcing methane and carbon dioxide emissions from a small city: influence of natural gas leakage and combustion. Environ. Pollut. 218, 102–111. https://doi.org/10.1016/j.envpol.2016.08.036.

Cicerone, R.J., Oremland, R.S., 1988. Biogeochemical aspects of atmospheric methane. Glob. Biogeochem. Cycles 2 (4), 299–327. https://doi.org/10.1029/GB002i004p00299.

Clark-Thorne, S.T., Yapp, C.J., 2003. Stable carbon isotope constraints on mixing and mass balance of CO_2 in an urban atmosphere: Dallas metropolitan area, Texas, USA. Appl. Geochem. 18, 75–95. https://doi.org/10.1016/S0883-2927(02)00054-9.

Dlugokencky, E., 2018. NOAA/ESRL. www.esrl.noaa.gov/gmd/ccgg/trends_ch4/.

Falge, E., Baldocchi, D., Olson, R., Anthoni, P., Aubinet, M., Bernhofer, C., Burba, G., Ceulemans, R., Clement, R., Dolman, H., Granier, A., Gross, P., Grünwald, T., Hollinger, D., Jensen, N.O., Katul, G., Keronen, P., Kowalski, A., Lai, C.T., Law, B.E., Meyers, T., Moncrieff, J., Moors, E., Munger, J.W., Pilegaard, K., Rannik, Ü., Rebmann, C., Suyker, A., Tenhunen, J., Tu, K., Verma, S., Vesala, T., Wilson, K., Wofsy, S., 2001. Gap filling strategies for defensible annual sums of net ecosystem exchange. Agric. For. Meteorol. 107, 43–69. https://doi.org/10.1016/S0168-1923(00)00225-2.

Foken, Th., Wichura, B., 1996. Tools for quality assessment of surface-based flux measurements. Agric. For. Meteorol. 78, 83–105. https://doi.org/10.1016/0168-1923(95)02248-1.

Gioli, B., Toscano, P., Lugato, E., Matese, A., Miglietta, F., Zaldei, A., Vaccari, F.P., 2012. Methane and carbon dioxide fluxes and source partitioning in urban areas: the case study of Florence, Italy. Environ. Pollut. 164, 125–131. https://doi.org/10.1016/j.envpol.2012.01.019.

Gioli, B., Gualtieri, G., Busillo, C., Calastrini, F., Zaldei, A., Toscano, P., 2015. Improving high resolution emission inventories with local proxies and urban eddy covariance flux measurements. Atmos. Environ. 115, 246–256. https://doi.org/10.1016/j.atmosenv.2015.05.068.

Górka, M., Lewicka-Szczebak, D., 2013. One-year spatial and temporal monitoring of concentration and carbon isotopic composition of atmospheric CO_2 in a Wrocław (SW Poland) city area. Appl. Geochem. 35, 7–13. https://doi.org/10.1016/j.apgeochem.2013.05.010.

Górka, M., Lewicka-Szczebak, D., Fuß, R., Jakubiak, M., Jędrysek, M.O., 2014. Dynamics and origin of atmospheric CH_4 in a Polish metropolitan area characterized by wetlands. Appl. Geochem. 45, 72–81. https://doi.org/10.1016/j.apgeochem.2014.03.007.

Graf, A., van de Boer, A., Moene, A., Vereecken, H., 2014. Intercomparison of methods for the simultaneous estimation of zero-plane displacement and aerodynamic roughness length from single-level eddy-covariance data. Bound.-Layer Meteorol. 151 (2), 373–387. https://doi.org/10.1007/s10546-013-9905-z.

Grimmond, C.S.B., King, T.S., Cropley, F.D., Nowak, D.J., Souch, C., 2002. Local-scale fluxes of carbon dioxide in urban environments: methodological challenges and results from Chicago. Environ. Pollut. 116, S243–S254. https://doi.org/10.1016/S0269-7491(01)00256-1.

Gualtieri, G., Crisci, A., Tartaglia, M., Toscano, P., Vagnoli, C., Andreini, B.P., Gioli, B., 2014. Analysis of 20-year air quality trends and relationship with emission data: the case of Florence (Italy). Urban Clim. 10, 530–549. https://doi.org/10.1016/j.uclim.2014.03.010.

Helfter, C., Tremper, A.H., Halios, C.H., Kotthaus, S., Bjorkegren, A., Grimmond, C.S.B., Barlow, J.F., Nemitz, E., 2016. Spatial and temporal variabilty of urban fluxes of methane, carbon monoxide and carbon dioxide above London, UK. Atmos. Chem. Phys. 16, 10543–10557. https://doi.org/10.5194/acp-16-10543-2016.

Hoornweg, D., Sugar, L., Lorena, C., Gómez, T., 2011. Cities and greenhouse gas emissions: moving forward. Environment & Urbanization 23 (1), 207–227. https://doi.org/10.1177/0956247810392270.

Hsieh, C.I., Katul, G., Chi, T., 2000. An approximate analytical model for footprint estimation of scalar fluxes in thermally stratified atmospheric flows. Adv. Water Resour. 23 (7), 765–772. https://doi.org/10.1016/S0309-1708(99)00042-1.

Huang, L., Wu, J., Yan, L., 2015. Defining and measuring urban sustainability: a review of indicators. Landsc. Ecol. 30, 1175–1193. https://doi.org/10.1007/s10980-015-0208-2.

Keeling, C.D., 1958. The concentration and isotopic abundances of atmospheric carbon dioxide in rural areas. Geochim. Cosmochim. Acta 13, 322–334. https://doi.org/10.1016/0016-7037(58)90033-4.

Keeling, C.D., 1961. The concentration and isotopic abundances of carbon dioxide in rural and marine air. Geochim. Cosmochim. Acta 24, 277–298. https://doi.org/10.1016/0016-7037(61)90023-0.

Keeling, C.D., Piper, S.C., Bacastow, R.B., Wahlen, M., Whorf, T.P., Heimann, M., Meijer, H.A., 2005. Atmospheric CO_2 and $^{13}CO_2$ exchange with the terrestrial biosphere and oceans from 1978 to 2000: observations and carbon cycle implications. In: Ehleringer, J.R., Cerling, T.E., Dearing, M.D. (Eds.), A History of Atmospheric CO_2 and its Effects on Plants, Animals, and Ecosystems. Springer Verlag, New York, pp. 83–113.

Levin, I., Bergamaschi, P., Dörr, H., Trapp, D., 1993. Stable isotopic signature of methane from major sources in Germany. Chemosphere 26 (1–4), 161–177. https://doi.org/10.1016/0045-6535(93)90419-6.

Lloyd, J., Farquhar, G.D., 1994. ^{13}C discrimination during CO_2 assimilation by the terrestrial biosphere. Oecologia 99, 201–215. https://doi.org/10.1007/BF00627732.

Lowry, D., Holmes, C.W., Rata, N.D., O'Brien, P., Nisbet, E.G., 2001. London methane emissions: use of diurnal changes in concentration and $\delta^{13}C$ to identify urban sources and verify inventories. J. Geophys. Res. 106 (D7), 7427–7448. https://doi.org/10.1029/2000JD900601.

Matese, A., Gioli, B., Vaccari, F.P., Zaldei, A., Miglietta, F., 2009. Carbon dioxide emissions of the city center of Firenze, Italy: measurement, evaluation, and source partitioning. J. Appl. Meteorol. Climatol. 48, 1940–1947. https://doi.org/10.1175/2009JAMC1945.1.

McKain, K., Down, A., Raciti, S.M., Budney, J., Hutyra, L.R., Floerchinger, C., Herndon, S.C., Nehrkorn, T., Zahniser, M.S., Jackson, R.B., Phillips, N., Wofsy, S.C., 2015. Methane emissions from natural gas infrastructure and use in the urban region of Boston, Massachusetts. PNAS 112 (7), 1941–1946. https://doi.org/10.1073/pnas.1416261112.

Meerow, S., Newell, J.P., Stults, M., 2016. Defining urban resilience: a review. Landsc. Urban Plan. 147, 38–49. https://doi.org/10.1016/j.landurbplan.2015.11.011.

Moore, C.J., 1986. Frequency response corrections for eddy correlation systems. Bound.-Layer Meteorol. 37, 17–35. https://doi.org/10.1007/BF00122754.

Moore, J., Jacobson, A.D., 2015. Seasonally varying contributions to urban CO_2 in the Chicago, Illinois, USA region: insights from a high-resolution CO_2 concentration and $\delta^{13}C$ record. Elementa: Science of the Anthropocene 3, 000052. https://doi.org/10.12952/journal.elementa.000052.

Nakagawa, F., Tsunogai, U., Komatsu, D.D., Yamada, K., Yoshida, N., Moriizumi, J., Nagamine, K., Iida, T., Ikebe, Y., 2005. Automobile exhaust as a source of ^{13}C- and D-enriched atmospheric methane in urban areas. Org. Geochem. 36, 727–738. https://doi.org/10.1016/j.orggeochem.2005.01.003.

Pang, J., Wen, X., Sun, X., 2016. Mixing ratio and carbon isotopic composition investigation of atmospheric CO_2 in Beijing, China. Sci. Total Environ. 539, 322–330. https://doi.org/10.1016/j.scitotenv.2015.08.130.

Papale, D., Reichstein, M., Aubinet, M., Canfora, E., Bernhofer, C., Kutsch, W., Longdoz, B., Rambal, S., Valentini, R., Vesala, T., Yakir, D., 2006. Towards a standardized processing of net ecosystem exchange measured with eddy covariance technique: algorithms and uncertainty estimation. Biogeosciences 3, 571–583. https://doi.org/10.5194/bg-3-571-2006.

Pataki, D.E., Bowling, D.R., Ehleringer, J.R., 2003a. Seasonal cycle of carbon dioxide and its isotopic composition in an urban atmosphere: anthropogenic and biogenic effects. J. Geophys. Res. 108 (D23), 4735. https://doi.org/10.1029/2003JD003865.

Pataki, D.E., Ehleringer, J.R., Flanagan, L.B., Yakir, D., Bowling, D.R., Still, C.J., Buchmann, N., Kaplan, J.O., Berry, J.A., 2003b. The application and interpretation of Keeling plots in terrestrial carbon cycle research. Glob. Biogeochem. Cycles 17 (1), 1022. https://doi.org/10.1029/2001GB001850.

Pawlak, W., Fortuniak, K., 2016. Eddy covariance measurements of the net turbulent methane flux in the city centre – results of 2-year campaign in Łódź, Poland. Atmos. Chem. Phys. 16, 8281–8294. https://doi.org/10.5194/acp-16-8281-2016.

Pichler, P.P., Zwickel, T., Chavez, A., Kretschmer, T., Seddon, J., Weisz, H., 2017. Reducing urban greenhouse gas footprints. Sci. Rep. 7, 14659. https://doi.org/10.1038/s41598-017-15303-x.

Quay, P.D., King, S.L., Lansdown, J.M., Wilbur, D.O., 1988. Isotopic composition of methane released from wetlands: implications for the increase in atmospheric methane. Glob. Biogeochem. Cycles 2 (4), 385–397. https://doi.org/10.1029/GB002i004p00385.

R Core Team, 2017. R: A Language and Environment for Statistical Computing. https://www.R-project.org/.

Regione Toscana, 2010. Inventario regionale delle sorgenti di emissione in aria ambiente – IRSE. Aggiornamento all'anno 2010. Direzione Generale Politiche Territoriali Ambientali e per la Mobilità, Settore Energia, tutela della qualità dell'aria e dall'inquinamento elettromagnetico e acustico, Firenze, Italy.

Running, S.W., Nemani, R.R., Heinsch, F.A., Zhao, M., Reeves, M., Hashimoto, H., 2004. A continuous satellite-derived measure of global terrestrial primary production. BioScience 54 (6), 547–560. https://doi.org/10.1641/0006-3568(2004)054[0547,ACSMOG]2.0.CO;2.

Schwietzke, S., Sherwood, O.A., Bruhwiler, L.M.P., Miller, J.B., Etiope, G., Dlugokencky, E.J., Englund Michel, S., Arling, V.A., Vaughn, B.H., White, J.W.C., Tans, P.P., 2016. Upward revision of global fossil fuel methane emissions based on isotope database. Nature 538, 88–91. https://doi.org/10.1038/nature19797.

Sherwood, O.A., Schwietzke, S., Arling, V.A., Etiope, G., 2017. Global inventory of gas geochemistry data from fossil fuel, microbial and burning sources, version 2017. Earth System Science Data 9, 639–656. https://doi.org/10.5194/essd-9-639-2017.

Townsend-Small, A., Tyler, S.C., Pataki, D.E., Xu, X., Christensen, L.E., 2012. Isotopic measurements of atmospheric methane in Los Angeles, California, USA: influence of "fugitive" fossil fuel emissions. J. Geophys. Res. 117, D07308. https://doi.org/10.1029/2011JD016826.

United Nations Population Division, 2018. World urbanization prospects: the 2018 revision. United Nations Department of Economic and Social Affairs (UN DESA)https://population.un.org/wup/Publications/.

Vaccari, F.P., Gioli, B., Toscano, P., Perrone, C., 2013. Carbon dioxide balance assessment of the city of Florence (Italy), and implications for urban planning. Landsc. Urban Plan. 120, 138–146. https://doi.org/10.1016/j.landurbplan.2013.08.004.

Velasco, E., Roth, M., 2010. Cities as net sources of CO_2: review of atmospheric CO_2 exchange in urban environments measured by eddy covariance technique. Geogr. Compass 4 (9), 1238–1259. https://doi.org/10.1111/j.1749-8198.2010.00384.x.

Velasco, E., Pressley, S., Allwine, E., Westberg, H., Lamb, B., 2005. Measurement of CO_2 fluxes from the Mexico City urban landscape. Atmos. Environ. 39, 7433–7446. https://doi.org/10.1016/j.atmosenv.2005.08.038.

Velasco, E., Pressley, S., Grivicke, R., Allwine, E., Coons, T., Foster, W., Jobson, B.T., Westberg, H., Ramos, R., Hernández, F., Molina, L.T., Lamb, B., 2009. Eddy covariance flux measurements of pollutant gases in urban Mexico City. Atmos. Chem. Phys. 9, 7325–7342. https://doi.org/10.5194/acp-9-7325-2009.

Zazzeri, G., Lowry, D., Fisher, R.E., France, J.L., Lanoisellé, M., Grimmond, C.S.B., Nisbet, E.G., 2017. Evaluating methane inventories by isotopic analysis in the London region. Sci. Rep. 7, 4854. https://doi.org/10.1038/s41598-017-04802-6.

Zimnoch, M., 2009. Stable isotope composition of carbon dioxide emitted from anthropogenic sources in the Kraków region, Southern Poland. Nukleonika 54 (4), 291–295.

Zobitz, J.M., Keener, J.P., Schnyder, H., Bowling, D.R., 2006. Sensitivity analysis and quantification of uncertainty for isotopic mixing relationships in carbon cycle research. Agric. For. Meteorol. 136, 56–75. https://doi.org/10.1016/j.agrformet.2006.01.003.